

Spatiotemporal Forward Solution of the EEG and MEG Using Network Modeling

Viktor K. Jirsa*, Kelly J. Jantzen, Armin Fuchs, and J. A. Scott Kelso

Abstract—Dynamic systems have proven to be well suited to describe a broad spectrum of human coordination behavior such synchronization with auditory stimuli. Simultaneous measurements of the spatiotemporal dynamics of electroencephalographic (EEG) and magnetoencephalographic (MEG) data reveals that the dynamics of the brain signals is highly ordered and also accessible by dynamic systems theory. However, models of EEG and MEG dynamics have typically been formulated only in terms of phenomenological modeling such as fixed-current dipoles or spatial EEG and MEG patterns. In this paper, it is our goal to connect three levels of organization, that is the level of coordination behavior, the level of patterns observed in the EEG and MEG and the level of neuronal network dynamics. To do so, we develop a methodological framework, which defines the spatiotemporal dynamics of neural ensembles, the neural field, on a sphere in three dimensions. Using magnetic resonance imaging we map the neural field dynamics from the sphere onto the folded cortical surface of a hemisphere. The neural field represents the current flow perpendicular to the cortex and, thus, allows for the calculation of the electric potentials on the surface of the skull and the magnetic fields outside the skull to be measured by EEG and MEG, respectively. For demonstration of the dynamics, we present the propagation of activation at a single cortical site resulting from a transient input. Finally, a mapping between finger movement profile and EEG/MEG patterns is obtained using Volterra integrals.

Index Terms—Dynamics, EEG, forward solution, MEG, modeling, network.

I. INTRODUCTION

NONINVASIVE techniques such as functional magnetic resonance imaging (fMRI), electroencephalography (EEG), and magnetoencephalography (MEG) provide entry points to human brain dynamics for the study of human behavior and cognition, as well as for clinical purposes. Each of these imaging technologies provides spatiotemporal information about the on-going neural activity in the cortex. Analysis techniques of experimental spatiotemporal data typically involve the identification of foci of activity such as single- or multiple-dipole localization (see [53] and [64] for an overview) in a three-dimensional (3-D) volume. Other

techniques emphasize the pattern approach which aims at the identification of activity patterns defined on the two-dimensional (2-D) surface spanned by the EEG and MEG detectors. These remain somewhat invariant during the time course of brain activity and typically minimize a postulated norm such as the Gaussian variance [principal component analysis (PCA)] [17], [40], [46] or non-Gaussian statistical independence [independent component analysis (ICA)] [50]. The latter may also be derived from a Bayesian framework [44]. Signal source projection (SSP) [62] provides a decomposition into patterns of activity which are physiologically or anatomically meaningful, by these means, however, restricting the possible solution space to the experimenters expectations. Similarly, dual space projections provide a decomposition into spatial patterns which are meaningful with respect to dynamics such as a maximal correlation with a peripheral signal [18]. More ambitious techniques wish not only to decompose the spatiotemporal dynamics into meaningful patterns, but also identify equations which govern the dynamics of these patterns [7], [8], [32], [47], [48], [63]. Unfortunately, the successful application of these techniques has been limited to special cases in which the majority of the observed dynamics has already been well understood [32]. Spatiotemporal activity propagation of electro- and magnetoencephalographic signals has been represented by discretely coupled oscillator models (see [64, chapter on source modeling]) representing dipole sources. Spatially and temporally continuous models, so-called neural fields, were formulated by Wilson and Cowan [67], [68], Nunez [54], and Amari [2] in the 1970s. With improving imaging techniques and the development of MEG, these types of models experienced a renaissance [15], [33], [49], [57], [69]. These models are based on coupled neural ensembles in a spatially continuous representation using integral equations involving a time delay via propagation. Jirsa and Haken [33] generalized and unified the earlier models by Wilson and Cowan [67], [68] and Nunez [54] and demonstrated that they describe the same system. The modeling on these different levels of organization has been phenomenological, i.e., only partially taking into account the specific neurobiological nature of the measured signal and its underlying mechanisms of generation. Each level of description has been tackled separately, never in unison with other fields of research and typically involving the application of strong simplifications. For example, the physiologically motivated neural field dynamics describes current flow perpendicular to the cortical sheet, but it is normally compared to the patterns of electric scalp potential measured by EEG. The latter patterns' dynamics is certainly related to the dynamics of the neural activations along the cortex, but not identical. Further, Steyn-Ross

Manuscript received November 1, 2–2001; revised February 26, 2002. This research was supported in part by the National Institute of Neurological Disorders and Stroke (NINDS) under Grant NS-39845, in part by the National Institute of Mental Health (NIMH) under Grant MH-42900 and Grant MH-01386, and in part by the Human Frontier Sciences Program. *Asterisk indicates corresponding author.*

*V. K. Jirsa is with the Center for Complex Systems and Brain Sciences, Florida Atlantic University, 777 Glades Road, Boca Raton, FL 33431 USA (e-mail: jirsa@walt.ccs.fau.edu).

K. J. Jantzen, A. Fuchs, and J. A. S. Kelso are with the Center for Complex Systems and Brain Sciences, Florida Atlantic University, Boca Raton, FL 33431 USA.

Publisher Item Identifier S 0278-0062(02)05534-9.

et al. [61] explain a hysteresis phenomenon called ‘biphasic response’ in the clinical human EEG during anesthesia. Their underlying neural model is based upon Liley’s work [49] using a spatially uniform activity distribution in one dimension with a connectivity distribution which falls off exponentially, independent of the cortical location. Jirsa *et al.* [35] also applied a one-dimensional (1-D) model, but allowed for varying spatial structure in the activity distributions. Here, by applying neural field equations to a bimanual coordination situation, they predicted the spatiotemporal dynamics observed in the MEG and confirmed these experimentally. A set of equations, governing human bimanual coordination [21], was derived from these neural field equations. This connection between spatiotemporal brain dynamics and behavioral dynamics has become possible through the notion of functional units [18], [33], [35] that serve as interfaces between neural and behavioral signals. Despite these successes, the simplifications made in these approaches do not take into consideration a more detailed physiological and anatomical interpretation of the identified dynamic mechanisms.

In this paper, we develop a methodological approach that allows, at least for the type of behavioral experiments discussed here, for the connection of the dynamics of neural activity along the cortex to the dynamics of EEG and MEG patterns, as well as the dynamics observed in motor behavior. The conceptual steps are the following. We define a spatiotemporal neural field dynamics on a spherical geometry. This special choice of coordinate system allows us to treat the high-dimensional dynamics not only computationally, but also mathematically. Then, in consecutive steps, the neuronal dynamics is mapped onto the unfolded cortical surface, then on the folded cortical surface (thereby minimizing the spatial distortions), and finally on the EEG and MEG patterns on the scalp. The connection between neural and behavioral dynamics is achieved by a linear convolution of the behavioral signal with an integral kernel, that is a first-order Volterra integral. The analysis task is to identify the correct integral kernel. Our paper is organized as follows. First, we review the dynamics of coordination behavior and its neural correlates. Second, we discuss the foundation of neural field dynamics and develop a systematic treatment of functional units. Third, we elaborate the methodologies involved in traversing scales of organization from the level of neural ensemble to EEG and MEG. Finally, we discuss the example of neural field dynamics after an induced stimulus and provide an outlook to future work.

II. BRAIN AND BEHAVIOR CORRELATES OF COORDINATION

The coordination of rhythmic finger movements has developed to a paradigm in human coordination dynamics [39], [41]. Behaviors, such as synchronization of finger movements, can be either described by the individual components, such as the positions of the finger tips, or by the equivalent movement patterns, such as the symmetric and anti-symmetric patterns of finger movements [36]. The latter are also called in-phase and anti-phase patterns, respectively. Component and pattern description are entirely equivalent. In the simplest scenario, when the finger movements are restricted to a 1-D flexion and exten-

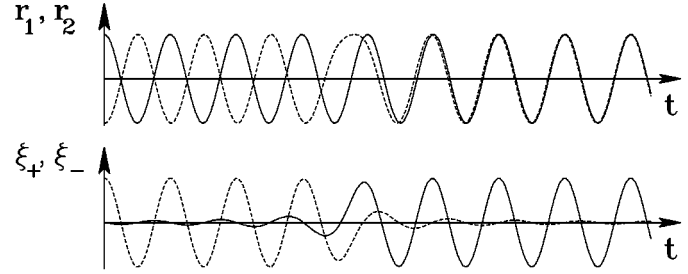


Fig. 1. An example of numerically generated time series of a phase transition: In the upper part, the left and right finger position r_1, r_2 initially oscillate in anti-phase, then a phase shift occurs and the finger positions move in-phase. Below, the same dynamics, but in terms of the movement patterns, $\xi_+(t) = (r_1 + r_2)/2$ and $\xi_-(t) = (r_1 - r_2)/2$, is shown.

sion of the index fingers, the left and right finger positions are the components and are given by the scalars $r_1(t)$ and $r_2(t)$, respectively. Both are obviously dependent on the time t . The movement patterns are then given by $\xi_+(t) = (r_1 + r_2)/2$ and $\xi_-(t) = (r_1 - r_2)/2$ where the plus sign denotes the symmetric coordination pattern and the minus sign the anti-symmetric pattern. Experimentally it turns out that when left and right fingers are moved anti-symmetrically, that is ξ_- has maximal amplitude and $\xi_+ = 0$ and the movement frequency is increased, a transition occurs from a dominating anti-symmetrical to a symmetrical pattern, that is ξ_+ obtains maximal amplitude and ξ_- becomes zero. See Fig. 1 for an illustration of this transition.

Such transitions, also called bifurcations, are a characteristic feature of complex systems capable of pattern formation. All phenomena known from phase transitions in physical systems, such as hysteresis for example, may also be found in behavioral pattern formation. Similar to our description of behavior, we wish to describe the spatiotemporal patterns observed using EEG and MEG during movement coordination as a pattern formation process. Each EEG or MEG sensor measures a time series $h_i(t)$ where i indexes the sensor. The individual measurements $h_i(t)$ of each sensor represent here the component level and may be arranged in a vector $\mathbf{H}(t) = (\cdots h_i(t) \cdots)$. The sensors are typically arranged in a helmet, as shown in the bottom right of Fig. 2 and span a 2-D surface Z over the skull. When this surface is unfolded, a so-called brain map or scalp topography is obtained for each point in time t : the measurements $h_i(t)$ are interpolated on the surface Z and color-coded to provide a spatially continuous representation of the EEG or MEG measurements. Accordingly, the discrete vector $\mathbf{H}(t)$ becomes a spatially continuous field $h(x, t)$ with $x \in Z$. When plotted for each time point, the resulting series of scalp topographies is called a space-time series. An example of a space-time series is shown for a unimanual coordination experiment on the bottom of Fig. 2, time increasing from top left to bottom right. A review of the results in Fig. 2 will serve to illustrate that phase transitions and pattern formation phenomena in behavior are strongly correlated with phase transitions and pattern formation phenomena in the EEG and MEG scalp topographies. During the coordination experiment, the subject was instructed to perform a right-handed finger movement in anti-phase with an auditory metronome starting at frequencies of 1 Hz and increasing in steps of 0.25 Hz. Intervals of constant stimulus fre-

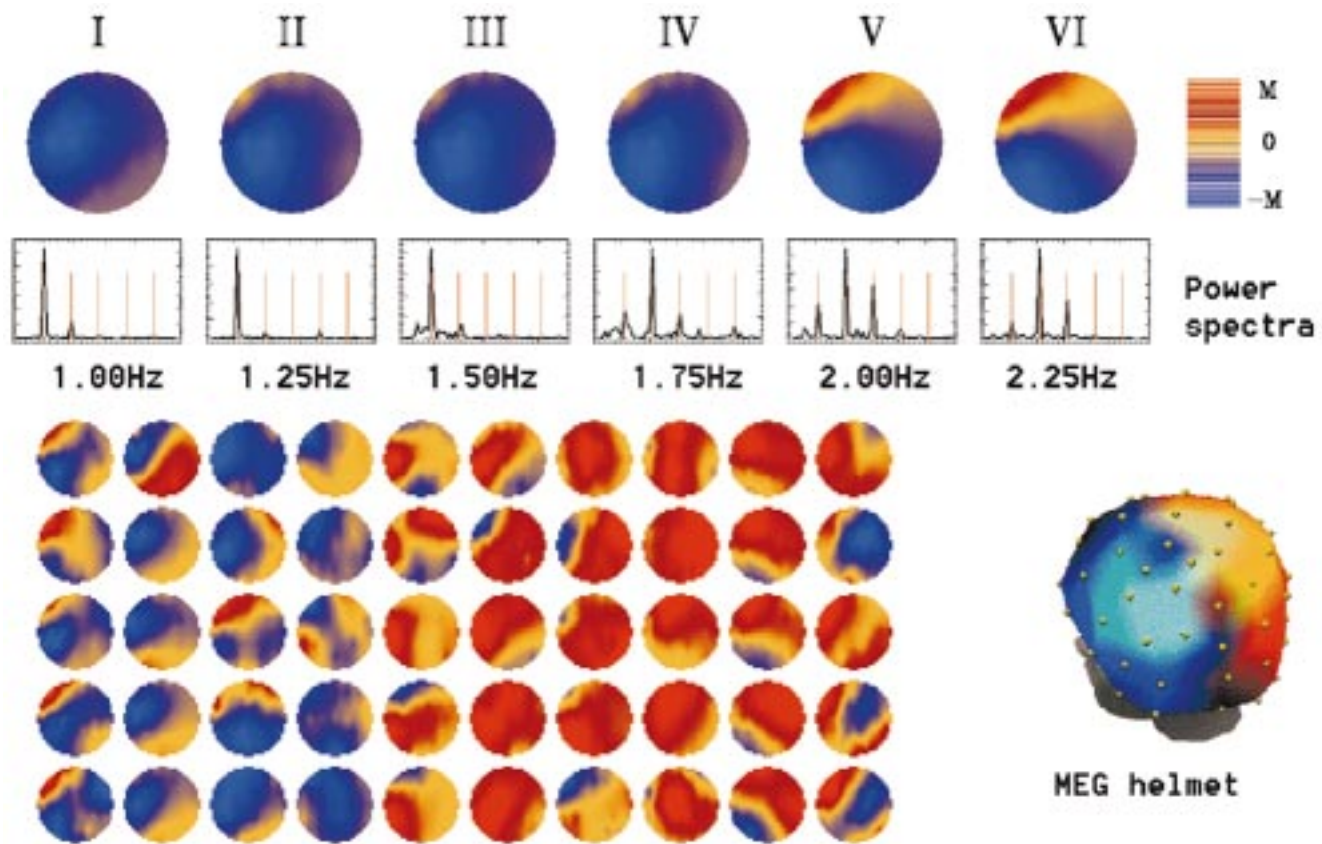


Fig. 2. Unimanual finger movement and its MEG. A 37-dimensional SQUID array was placed over the left hemisphere as illustrated in the bottom right graph. For six plateaus, corresponding to stimulation frequencies 1–2.25 Hz, the dominant spatial structure is plotted in the top row, together with its power spectrum. In the latter, the vertical red lines denote the stimulus frequency and its higher harmonics. The phase transition in behavior occurs on plateau IV, coincident with a change in the spatial patterns and the power spectra. An example space-time series of five cycles on plateau II is plotted in the bottom left.

quency are referred to as plateaus. Behaviorally, the subject underwent a transition from anti-phase movement to synchronization with the stimulus on plateau IV at a required rate of 1.75 Hz. During the experiment MEG was recorded from sensors located centrally over the primary motor and auditory areas of the left hemisphere, centered 2 cm from C3 (10–20 system) in the posterior direction. The SQUID system consists of 37 axially symmetric first-order gradiometers each 20 mm in diameter and spaced 22 mm apart. Each sensor had a sampling frequency of 862 Hz and a bandpass filter between 0.1 and 100 Hz. Analyses [17] showed that the first two spatial principal components (PCA) carry about 80% of the variance of the entire MEG signal and imply the presence of two spatial patterns dominating the space-time series of the scalp topographies. As shown in the first row of Fig. 2, the strongest PCA pattern of each plateau carries about 60% of the variance of the MEG signal. Before the transition, on plateaus I–III, the first pattern dominates. A transition occurs on plateau IV and a new pattern emerges on plateaus V and VI when the subject actually performs an in-phase motion. This transition from one pattern to the other pattern is accompanied by a transition in the frequency domain: On plateaus I through III, the observed MEG pattern oscillates mainly with the movement frequency and on plateaus V and VI mainly with twice the movement frequency. As an example of the spatiotemporal sequence for constant stimulus frequency, Fig. 2 shows five cycles of the measured MEG pat-

terns at different time instances during plateau II. This sequence clearly exhibits the dominance of the first pattern extracted in the earlier analysis, Fig. 2 (top left).

The vector $\mathbf{H}(t) = (\dots h_i(t) \dots)$ with the measurements $h_i(t)$ may be decomposed as

$$\mathbf{H}(t) = \xi_1(t)\mathbf{v}_1 + \xi_2(t)\mathbf{v}_2 + \mathbf{n}(t) \quad (1)$$

where $\mathbf{v}_1, \mathbf{v}_2$ are the time-independent spatial modes obtained from the PCA. Their time evolution is captured by the corresponding time-dependent coefficients $\xi_1(t), \xi_2(t)$. In the interpolated spatially continuous representation, (1) reads

$$h(x, t) = \xi_1(t)v_1(x) + \xi_2(t)v_2(x) + n(x, t). \quad (2)$$

The modes $\mathbf{v}_1, \mathbf{v}_2$ or $v_1(x), v_2(x)$ characterize the spatial patterns of the EEG and MEG and the time-dependent coefficients $\xi_1(t), \xi_2(t)$ characterize their dynamics. The remainder of the signal is captured by $\mathbf{n}(t)$ or $n(x, t)$. There is a variety of procedures available to extract patterns from a space-time series some of which have been mentioned in Section I. The particular choice depends on the question asked, for instance a PCA minimizes the variance of the measured signals under the condition of orthogonal patterns. In the present experiment a PCA has been chosen [17], but other techniques which do not require orthogonal patterns essentially provided the same results [32]. Because the contribution of the remainder of the signal, $\mathbf{n}(t)$, to the variance of the entire signal $\mathbf{H}(t)$ is small, we perform the

approximation $\mathbf{H}(t) \approx \xi_1(t)\mathbf{v}_1 + \xi_2(t)\mathbf{v}_2$. The space-time dynamics of $\mathbf{H}(t)$ may now be interpreted as a competition of two patterns $\mathbf{v}_1, \mathbf{v}_2$: Initially, the pattern \mathbf{v}_1 dominates, then a transition occurs and the pattern \mathbf{v}_2 takes over. The dynamics and transition of these patterns has been described as an interaction of their time-dependent coefficients $\xi_1(t), \xi_2(t)$ by means of ordinary differential equations of the form [31]

$$\ddot{\xi}_1 + f_1(\xi_1, \xi_2, \dot{\xi}_1, \dot{\xi}_2) = 0, \quad \ddot{\xi}_2 + f_2(\xi_1, \xi_2, \dot{\xi}_1, \dot{\xi}_2) = 0. \quad (3)$$

The dots denote the first and second time derivative, respectively. Models of this form are phenomenological and intended to capture the generic features of the system's dynamics, that is its bifurcation mechanism. Here, the task is to identify the typically nonlinear coupling terms f_1, f_2 . Phenomenological models are generic in its nature with respect to the dynamics, but their drawback is that no connection is being made to the underlying system which generates the measured signals. As a consequence, the mathematical coupling terms f_1, f_2 in the phenomenological model cannot be interpreted in physiological or anatomical terms. Neither is it strictly possible to identify the dynamics of these phenomenological models with the dynamics of the many physiologically motivated neuronal network models in the literature. Still, it is common practice to compare at least qualitatively the predictions of the physiological network models to EEG/MEG pattern dynamics.

We have addressed two levels of organization, the dynamics of patterns of behavior (such as the coordination of finger movements) and the dynamics of spatiotemporal patterns observed in the EEG and MEG. In Section III, we discuss the dynamics of physiologically motivated network models of neuronal activity. Then we develop the methodological steps needed to connect these levels of organization. An approach to the mapping of peripheral data (such as external stimuli, finger movements, etc.) to cortical activations is outlined and the algorithmic and computational requirements to map cortical activations (obtained from spatiotemporal network modeling) onto EEG and MEG signals are discussed.

III. METHODS

A. Neural Field Dynamics

We choose a macroscopic level of description, the neural ensemble, which is significant for the generation of EEG and MEG. The local field potential is generated by the simultaneous activity of thousands of neurons in the extracellular space of the cortical sheet. The resulting neural ensemble activity is understood to generate the EEG [16]. The simultaneous intracellular currents in the dendritic shafts of the neural ensembles generate the MEG [66]. The neuronal cell membranes, being good electrical insulators, guide the flow of both intracellular and extracellular currents and, thus, result in a current flow perpendicular to the cortical surface due to the perpendicular alignment and elongated shape of pyramidal neurons. The neural ensemble average of these currents results in the primary current density which is the site of the sources of brain activity and is denoted by the scalar so-called neural field $\psi(x, t)$ with x being the location on the 2-D folded cortical surface Γ and t

being the time. Note that, although the conversion of chemical gradients is due to diffusion, the primary current density $\psi(x, t)$ is determined largely by the cellular-level details of conductivity. The structure of our neural model is generic and found in most models describing neuronal activity: a firing rate of a neuronal ensemble at a location A is transmitted to a neuronal ensemble at a distant location B. Most models differ in variations of connectivity and inclusion of physiological detail. In the present neuronal field model, a time delay via transmission is considered due to the large spatiotemporal scales of interest. The following specific properties distinguish the present neuronal field model from most other approaches: Conversion operations [33] define mathematical relations between firing rates and local field potentials. Research by Freeman [16] and others [1], [60] showed in a variety of cortical areas that the neuronal firing rate and the local field potential are related in a well-defined way (the so-called conversion operations [16]): The conversion from local field potential to firing rate within a neuronal ensemble is sigmoidal. The inverse conversion, from firing rate to local field potential, is also sigmoidal, but constrained to a linear small-signal range. To capture the large spatial and temporal scales in EEG and MEG, the connectivity includes both, the short range intracortical fibers (excitatory and inhibitory), which typically have a length of 0.1 cm and the corticocortical (only excitatory) fibers with lengths ranging from about 1 cm to 20 cm [54]. Propagation along these long-range fibers may cause time delays up to 200 ms. The distribution of the intracortical fibers and, thus, the local connectivity, is homogeneous [6], whereas the distribution of the corticocortical fibers is not (estimates are that 40% of all possible corticocortical connections are realized for the visual areas in the primate cerebral cortex [13]). For these reasons an inhomogeneous interareal connectivity has to be allowed resulting in a translationally variant connectivity function $f(x, X) \neq f(x - X)$ with $x, X \in \Gamma$. External input $p(x, t)$ is realized such that afferent fibers make synaptic connections at a site on the cortical sheet Γ , whereas multiple inputs, such as an auditory, visual, or sensorimotor stimulus, lead to different sites on the cortical sheet. For its functional differentiation, the input $p(x, t)$ is also called a functional input unit [18] and will be discussed in more detail in the next section. The neural field dynamics may be written as

$$\psi(x, t) = \int_{\Gamma} dX f(x, X) \cdot S \left[\psi \left(X, t - \frac{|x - X|}{v} \right) + p \left(X, t - \frac{|x - X|}{v} \right) \right] \quad (4)$$

where $S[\cdot]$ represents the sigmoidal firing rate and v the propagation velocity along axonal fibers [33]. The neural field (4) is a nonlinear retarded integral equation with a spatially variant integral kernel, that is its dynamics is arbitrarily complex and will crucially depend on the choices of $f(x, X)$ and $p(x, t)$. To gain a first intuition of the neural field's dynamics, the following simplifications may be made (in this paragraph for illustrational purposes only): The cortical surface Γ is 1-D. The connectivity $f(x, X)$ is spatially invariant

$$f(x, X) = f(x - X) = \frac{1}{2\sigma} e^{-|x-X|/\sigma}. \quad (5)$$

Then, the method of Green's functions [33] may be applied which transforms (4) into the Fourier-space of physical space-time, reshuffles the terms in the equation and performs a back-transformation into physical space-time. The resulting equation is a nonlinear partial differential equation of the form

$$\ddot{\psi} + (\omega_0^2 - v^2 \Delta) \psi + 2\omega_0 \dot{\psi} = \left(\omega_0^2 + \omega_0 \frac{\partial}{\partial t} \right) \cdot S[\psi(x, t) + p(x, t)] \quad (6)$$

where $\omega_0 = v/\sigma > 0$ and the 1-D Laplacian $\Delta = \partial^2/(\partial x^2)$. Without any input, $p(x, t) = 0 \forall x, t$, the left-hand-side is a damped wave equation and has oscillatory properties. The spatially uniform pattern is generally stable, if the slope of the sigmoid function $S[\cdot]$ on the right-hand side of (6) is sufficiently small. Neurophysiologically, the steepness of the slope correlates with the excitability of the neural ensembles at the particular site, whereas the ensembles' excitability is typically determined by the biochemical environment such as the presence of neuromodulators. If the slope increases beyond a threshold, then the spatially uniform state is destabilized and wave propagation may occur. More complex connectivity functions than (5) result in an arbitrarily complex dynamics of (4). A first account of a nonhomogeneous connectivity function has been given in [37], [38]: Here, the authors embedded a fiber track connecting two distant areas into an otherwise homogeneously connected neural sheet. They showed that the system's spatiotemporal dynamics is guided through a series of bifurcations as the distance between the connected areas is varied. A representation of the dynamical system (4) as a partial differential equation turns out to be tedious and impractical due the nonlocal and spatially variant connectivity. Such connectivity functions displaying patches of enhanced connectivity between distinct areas have been reported experimentally in animal studies [6].

B. Functional Units

Functional units represent interfaces between the neocortex and peripheral (input and output) signals. A functional unit which maps EEG and MEG signals onto peripheral signals, e.g., the finger movement position $r(t)$, is called an output unit. Inversely, when an external signal is mapped onto an EEG or MEG signal, then the functional unit is an input unit. In the following, we will discuss the steps involved in the construction of a functional unit.

As a working hypothesis, a peripheral signal, here for concreteness the finger position $r(t)$, is assumed to be constructed as

$$r(t) = \int_{t_0}^t d\tau g(t - \tau) \int_Z dx v^{\text{out}}(x) h(x, \tau) \quad (7)$$

where t_0 is the initial time point of the measurements and $v^{\text{out}}(x)$ is a spatial pattern in the spatially continuous 2-D scalp topography in the space Z spanned by the EEG and MEG sensors as discussed in Section II. We further assume that the EEG and MEG dynamics during the finger movement may be represented by very few spatial patterns, typically one or two. This assumption has to be tested against the experiment (see [17], [32], [40], [41], [51], [65] for examples) by extracting the

spatial patterns using the earlier discussed mode decomposition techniques (PCA, dual space methods, SSP, etc). The integral kernel $g(t - \tau)$ is an unknown convolution function which we wish to determine. The finger position $r(t)$, the brain signal measurements $h(x, t)$ and the spatial patterns $v^{\text{out}}(x)$ are given by the experiment and, hence, are known variables. The mapping in (7) is the first term of a nonlinear Volterra series [59]. The truncation after the linear term may be motivated for rhythmic movements, since here the peripheral signals and the EEG and MEG activity of the functional units seem to be linearly related [17], [18], [43]. However, also higher order terms of the Volterra series may be considered (see [59] for a discussion of Volterra series). For brevity, we rewrite the time integral in (7) as a linear operator

$$\hat{L}s := \int_{t_0}^t d\tau g(t - \tau) s(\tau) \quad (8)$$

where $s(t)$ is an arbitrary time-dependent function. The inverse of the integral operator \hat{L} is a linear differential operator \hat{L}^{-1} with constant coefficients [11], [59]. Applying the inverse operator \hat{L}^{-1} in (7), we obtain

$$\hat{L}^{-1}r = \dots + c_2 \ddot{r}(t) + c_1 \dot{r}(t) + c_0 r(t) = \int_Z dx v^{\text{out}}(x) h(x, \tau) \quad (9)$$

where c_n , $n = 0, 1, 2, \dots$ are constant coefficients. Kelso *et al.* [43] found experimentally that the dynamics of the MEG signal $\mathbf{H}(t)$ during rhythmic finger movements may be decomposed into two spatial modes \mathbf{v}_1 and \mathbf{v}_2 . Here, again as in Section II, $\mathbf{H}(t)$ is a vector containing the MEG measurement of the sensors. The spatial modes \mathbf{v}_1 and \mathbf{v}_2 were obtained by minimizing a square error for the following decomposition [43], [18]

$$\mathbf{H}(t) = r(t)\mathbf{v}_1 + \dot{r}(t)\mathbf{v}_2 \quad (10)$$

with the finger position $r(t)$ and its velocity $\dot{r}(t)$. Note that the spatial modes \mathbf{v}_1 and \mathbf{v}_2 do not require to be orthogonal. Experimentally, it turns out that the velocity is the dominant contribution [43], i.e., the scalar products of the vectors obey $\mathbf{v}_1 \mathbf{v}_1 \ll \mathbf{v}_2 \mathbf{v}_2$. We multiply (10) by the dominating mode \mathbf{v}_2 and obtain

$$\mathbf{v}_2 \mathbf{H}(t) = r(t)\mathbf{v}_2 \mathbf{v}_1 + \dot{r}(t)\mathbf{v}_2 \mathbf{v}_2. \quad (11)$$

After division of (11) by $\mathbf{v}_2 \mathbf{v}_2$, a comparison with (9) provides the identification

$$\mathbf{v}^2 \longrightarrow v^{\text{out}}(x) \quad (12)$$

in the continuous limit and

$$c_0 = \frac{\mathbf{v}^1 \mathbf{v}^2}{\mathbf{v}^2 \mathbf{v}^2} \quad c_1 = 1 \quad c_2 = c_3 = \dots = 0. \quad (13)$$

There is one additional freedom, namely the scaling of either $r(t)$ or $h(x, t)$ which introduces the scaling parameter ϵ . With (13) we rewrite (9) as

$$\dot{r}(t) + c_0 r(t) = \epsilon \int_Z v^{\text{out}}(x) h(x, t) dx \quad (14)$$

where the left-hand side represents the intrinsic dynamics of the finger motion and the right-hand side the excitation by the brain signals, thus, we can interpret the finger movement as

an overdamped oscillator driven by the brain signals which are projected onto the functional output unit $v^{\text{out}}(x)$. The solution of (14) reads

$$r(t) = \epsilon \int_Z v^{\text{out}}(x) \int_{t_0}^t g(t-\tau) h(x, \tau) d\tau dx \quad (15)$$

with the transfer function

$$g(t-\tau) = e^{-c_0(t-\tau)}, \quad (16)$$

and the initial time point far in the past, i.e., $t_0 \approx -\infty$.

Until now the spatial component of a functional units has been identified with the spatial patterns \mathbf{v}_1 and \mathbf{v}_2 which are observed in the EEG/MEG and generated by time-dependent input signals (e.g., see [43]). This is due to the fact that the description and the modeling of EEG/MEG dynamics has been almost exclusively in terms of patterns rather than cortical sources. In the case of a finger movement, the dominating spatial pattern \mathbf{v}_2 corresponds to a dipolar pattern in the EEG/MEG located over the contralateral motor cortex and is shown in Fig. 3. Anatomically, these areas are defined via their afferent and efferent fibers connecting to the cortical sheet. The connection between cortical source currents $\psi(x, t)$ confined to the cortical surface Γ and the resulting EEG and MEG pattern $\mathbf{H}(t)$ spanning the interpolated surface Z is given by the forward propagator discussed in Section III-F. Equivalently, a functional input unit $p(x, t)$ (see [18] for a detailed treatment) is defined by its location $\beta(x)$ on the folded cortical sheet Γ and a time-dependent peripheral signal $r(t)$

$$p(x, t) = \beta(x) \int_{t_0}^t f(t-\tau) r(\tau) d\tau \quad (17)$$

where t_0 is the initial time point and $f(t-\tau)$ the to be determined convolution function. The cortical site $\beta(x)$ on the surface Γ and its location and orientation in the 3-D physical space (remember that the cortical surface Γ is a 2-D folded surface in the 3-D physical space!) determine the observable EEG and MEG pattern on the skull surface Z . This is known as the forward solution. When an input $r(t)$ arrives at the cortical site $\beta(x)$, $x \in \Gamma$, it excites the neural ensembles through (4), (17) and gives rise to spatiotemporal pattern formation along Γ . The forward solution generates the corresponding EEG and MEG patterns $h(x, t)$, $x \in Z$ for every point in time.

Our main results are (12), (13), (15), and (16). Here, (15) defines an explicit relation between the brain activity $h(x, t)$ measured by EEG/MEG and a rhythmic finger movement $r(t)$. Fig. 3 shows the reconstruction of the movement profile from experimentally obtained MEG activity according to (15). Here, subjects were instructed to coordinate the movement of their right (preferred) index finger with a visual metronome at a frequency of 1 Hz. Measures of finger displacement over time were obtained as pressure changes in an air cushion detected by transducers. During the experiment, the magnetic field generated by the on-going neural activity was measured using a 68-channel full-head magnetometer at a sampling frequency of 250 Hz. A total of 100 movement cycles was recorded and the brain signals in each sensor were averaged after artifact removal. Note the reconstructed movement profile fits the experimentally observed

movement particularly well in the active phase represented by its positive flank. The discrepancies mainly occur after peak displacement and are probably due to the sensory feedback which is not accounted for by (15).

C. Neural Field Dynamics on a Sphere

We wish to obtain a simple representation of the neural field dynamics (4) on a closed 2-D surface. The spherical geometry is an excellent candidate coordinate system because it has a simple parametrization. Spatial patterns may be decomposed into spherical harmonics which often provide a basis for a lower dimensional mathematical description of an otherwise complex dynamics. But, also, numerical algorithms benefit from a decomposition into spherical harmonics and may reduce the computation time needed for the integration of systems described by neural fields. For these reasons, we define the neural field (4) in two dimensions with spherical boundary conditions. For a homogeneous, exponentially decaying connectivity function [such as (5), but 2-D], the corresponding partial differential equation can be determined

$$\left(\frac{\partial^2}{\partial t^2} + 2\omega \frac{\partial}{\partial t} + \omega_0^2 - v^2 \Delta \right)^{3/2} \psi(x, t) = \left(\omega_0^3 + \omega_0^2 \frac{\partial}{\partial t} \right) \cdot S [\psi(x, t) + p(x, t)] \quad (18)$$

with the 2-D Laplacian acting on $\psi(x, t)$, $x \in \Gamma$. The details of the differential operators on the left-hand side of (18) depend on the spatial decay of the connectivity. However, these details are not significant for large scale pattern formation as shown by Haken [24]. For the purpose of calculating dynamics on the brain, each cortical hemisphere is represented in a spherical geometry and its dynamics is defined by (4) or (18), respectively. The two spheres interact by two means: through callosal pathways connecting the two spheres and through afferent fibers (crossing and noncrossing) from the periphery. Subcortical regions such as the brainstem are not included. Should heterogeneous fiber pathways be included also, then the integral representation given by (4) is used and two types of pathways distinguished: 1) The callosal fiber system from one sphere to another is treated in a manner equivalent to peripheral afferents; 2) Other heterogeneous pathways are included in the connectivity function $f(x, X)$. Note that heterogeneous pathways contribute strongly to the dynamics on all scales of organization; even local changes of connectivity have recently been shown to result in a major reorganization of brain activity [37], [38].

D. Unfolding of the Cortical Sheet and its Spherical Representation

In order to equate the distribution of neural fields with actual cortical structure, a mapping between the spherical surface and the cortical surface is required. Several steps are undertaken to complete this mapping. All of the described procedures were performed using the Freesurfer software package developed by Dale and colleagues [10], [12]. The first step is the segmentation of the brain structure and the definition of the gray-white matter boundary within each hemisphere. This step allows for the description of the cortical surface by a mesh defined by a

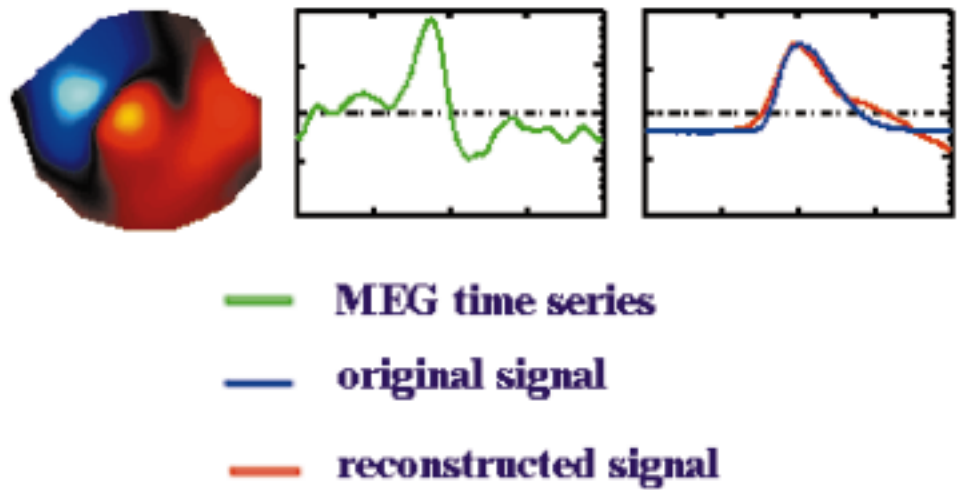


Fig. 3. Functional unit of a right-handed finger movement. The spatial MEG pattern, that is $v^{out}(x)$, is shown on the left which represents the dominant spatial structure present in the MEG signals obtained from a 64-sensor full-head detector. Here, the unfolded scalp topography is shown with the nose on the top, left ear is left, right is ear right. In the middle, the time series obtained from the projection onto the functional unit, $\int_{\mathcal{Z}} dx v^{out}(x)h(x, t)$, is shown. On the right, the time series showing the experimental finger movement $r(t)$ is plotted in blue and the reconstruction using the functional unit [see (15)] is plotted in red. All the time series range from -500 ms to 500 ms with maximum flexion at $t = 0$.

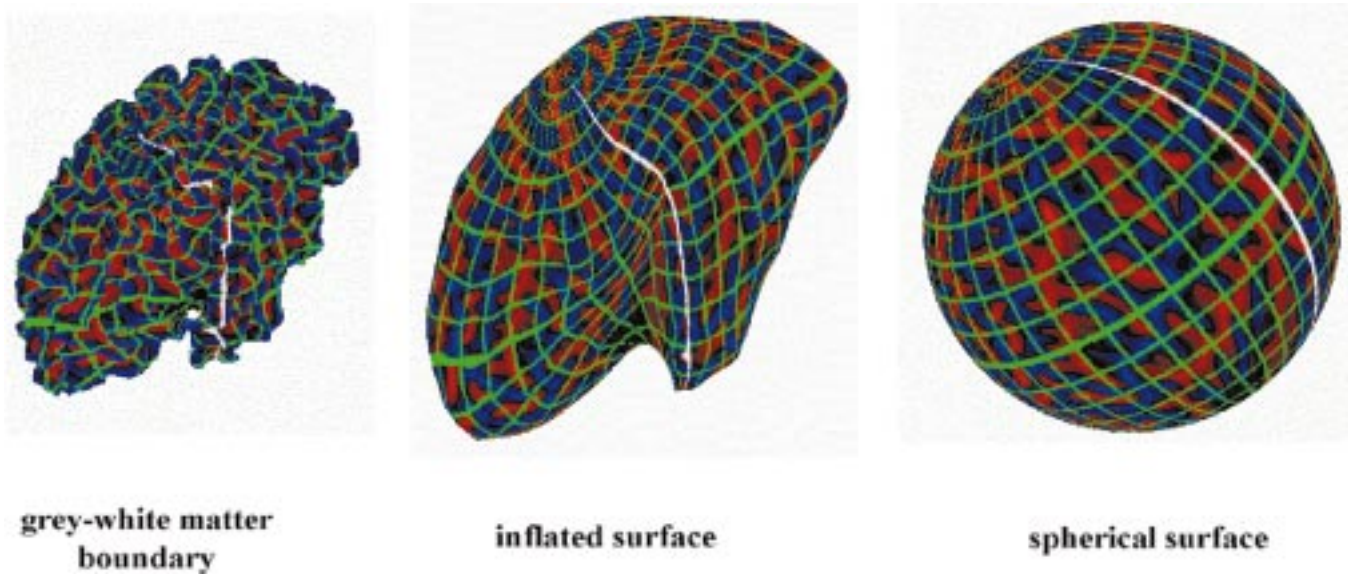


Fig. 4. Inflating the surface, representing the gray-white matter boundary and mapping onto a sphere. From right to left, the sequence shows how a spherical coordinate grid gets folded into the fissures.

set of vertices and polygons. The second step involves the inflation of the cortical surface to produce a closed surface that has minimal folding but also minimizes any distortion in the relative location between cortical locations (see middle image of Fig. 4). This step eliminates the difficulty of visualizing cortical activity within sulci. The final step is to transform this shape onto a spherical representation while maintaining as much of the spatial relation as possible by preserving the metric properties of the surface while minimizing the local curvature. With this procedure, any point on the folded cortex can be addressed using any number of coordinate systems via its isometric location on the neural sphere. Both transformations, forward and backward, are well defined and their product yields the identity. Fig. 4 gives an impression of this process by showing the three surfaces with the cortical surface color coded in red and blue

according to curvature. A spherical coordinate grid is plotted in green with the line of zero longitude in white. The resulting meshes are extremely dense typically involving on the order of 150 000 vertices for the representation of a single hemisphere. For the purpose of computational frugality, we decimated this tessellation to a more manageable number of vertices and corresponding polygons, 4512 and 9022, respectively.

E. Representation of Neural Fields on the Folded Cortex

In the previous section, we described how each hemisphere was expanded and warped onto a sphere. As a result of this transformation, each sampled vertex on the folded cortical surface has a corresponding vertex located on the surface of a sphere. In addition to this one-to-one mapping between the vertices

defining both the surface of the cortex and a sphere, the connectivity of the polygons (i.e., how the vertices are connected) remains the same across this transformation. The description of activity on the surface of the spherical hemisphere is automatically mapped onto the surface of the cortical representation. The task, therefore, simplifies to the mapping of the activity onto the surface of an irregularly sampled sphere. This is a simple matter, however, because the neural field is continuous across the sphere on which it is generated and therefore, can be sampled at any arbitrary point. The mesh vertices of the cortical sphere are easily converted to spherical coordinates and the value at the corresponding location of the neural field sphere is assigned. Caution has to be taken, though, when the space-time structure of the neural field dynamics on the sphere is compared with the one on the folded cortex. The nonconformal mapping of the Freesurfer software alters the distances between adjacent vertex points and, hence, the neural field dynamics. Fischl *et al.* [12] report an average local error of 20% between folded cortical and spherical coordinate system. In numerical simulations of neural fields that were homogeneously connected, we did not find any obvious discrepancies between the dynamics in both systems which is probably a consequence of the integration process in (4) resulting in an averaging of the error. Research of detailed error calculations of the space-time structure is on-going.

For graphical presentation, the field distribution over the cortical surface can be represented as a set of color values scaled between the maximum and minimum field strength. Changes in this color representation over time then give a temporal depiction of how the field dynamics unfold on the actual cortical surface. However, in order to calculate the forward solution using these current densities we need the additional information about the direction of current flow at each vertex location and each point in time. The generation of local field potentials within the cortex is dominated by activity in ensembles of pyramidal cells, which are oriented perpendicular to the cortical surface. It is possible, therefore, to model the direction of instantaneous current flow in a small cortical region as a normal vector on the mesh surface. The orientation of the vector gives the direction of current flow and the length of the vector gives the current strength. For the purpose of mapping neural activations onto the representation of the cortical surface a vector oriented normal to the polygon surface was computed for each mesh vertex. These vectors were then normalized to a length of one and scaled by the amount of neural activation at each time point. Because the direction of current flow is given by the orientation of the cellular generators, orientation of these vectors does not change over time (see Section III-F for details). Instantaneous current flow is always represented by vectors oriented orthogonal to the cortical surface while the propagation of current flow across the cortical surface is modeled as changes in the absolute and relative strengths of these vectors over time.

F. Forward Solution of the EEG and MEG

At this stage we have a representation of the current distribution in the 3-D physical space $x \in \mathcal{R}^3$ and its evolution over time t . To make a comparison with experimental data, the forward solutions of the scalar electric potential $V(x)$ on the skull surface and of the magnetic field vector $\mathbf{B}(x)$ at the detector

locations have to be calculated. Here, it is useful to divide the current density vector $\mathbf{J}(x)$ produced by neural activity into two components. The volume or return current density, $\mathbf{J}^v(x) = \sigma(x)\mathbf{E}(x)$, is passive and results from the macroscopic electric fields $\mathbf{E}(x)$ acting on the charge carriers in the conducting medium with the macroscopic conductivity $\sigma(x)$. The primary current density is the site of the sources of brain activity and is approximately identical to the neural field $\psi(x, t)$, because, although the conversion of chemical gradients is due to diffusion, the primary currents are determined largely by the cellular-level details of conductivity. The current flow is perpendicular to the cortical surface due to the perpendicular alignment and elongated shape of pyramidal neurons. In the quasi-static approximation of the Maxwell equations, the electric field becomes $\mathbf{E} = -\nabla V$ where ∇ is the Nabla-operator $(\dots \partial/\partial x \dots)^T$. The current density \mathbf{J} is

$$\mathbf{J}(x) = \psi(x, t)\mathbf{n}(x) + \sigma(x)\mathbf{E}(x) = \psi(x, t)\mathbf{n}(x) - \sigma(x)\nabla V(x) \quad (19)$$

where $\mathbf{n}(x)$ is the cortical surface normal vector at location x .

The forward problem of the EEG and MEG is the calculation of the electric potential $V(x)$ on the skull and the magnetic field $\mathbf{B}(x)$ outside the head from a given primary current distribution $\psi(x, t)\mathbf{n}(x)$. The sources of the electric and magnetic fields are both, primary and return currents. The situation is complicated by the fact that the present conductivities such as the brain tissue and the skull differ by the order of 100. Following the lines of Hämäläinen *et al.* [26], [27] and using the Ampère-Laplace law, the forward MEG solution is obtained by the volume integral

$$\mathbf{B}(x) = \frac{\mu_0}{4\pi} \int (\psi(x', t)\mathbf{n}(x') + V(x')\nabla'\sigma(x')) \times \frac{x - x'}{|x - x'|^3} dv' \quad (20)$$

where dv' is the volume element, ∇' the Nabla-operator with respect to x' , and μ_0 the magnetic vacuum permeability. The forward EEG solution is given by the boundary problem

$$\nabla \cdot (\sigma(x)\nabla V(x)) = \nabla \cdot (\psi(x, t)\mathbf{n}(x)) \quad (21)$$

which is to be solved numerically for an arbitrary head shape, typically using boundary element techniques as presented in [26], [27]. In particular, these authors showed that for the computation of neuromagnetic and neuroelectric fields arising from cortical sources, it is sufficient to replace the skull by a perfect insulator and therefore, to model the head as a bounded brain-shaped homogeneous conductor. Three surfaces, S_1 , S_2 , and S_3 , have to be considered at the scalp-air, the skull-scalp, and the skull-brain interface, respectively, whereas the latter provides the major contribution to the return currents. The 3-D geometry of these surfaces can be obtained from MRI scans. The inverse problem of the EEG and MEG is to estimate the cerebral current sources underlying the measurements. It was shown by Helmholtz in 1853 that a current distribution inside a conductor cannot be retrieved uniquely from knowledge of the electromagnetic fields outside. Hence, the inverse problem has to be constrained in order to provide reasonable estimates of the source locations. Typical constraints are assumptions about the type of the sources, such as single or multiple dipoles which may be either spatially fixed or rotating. Beam-forming approaches which focus on cortical regions of interest or other biases such

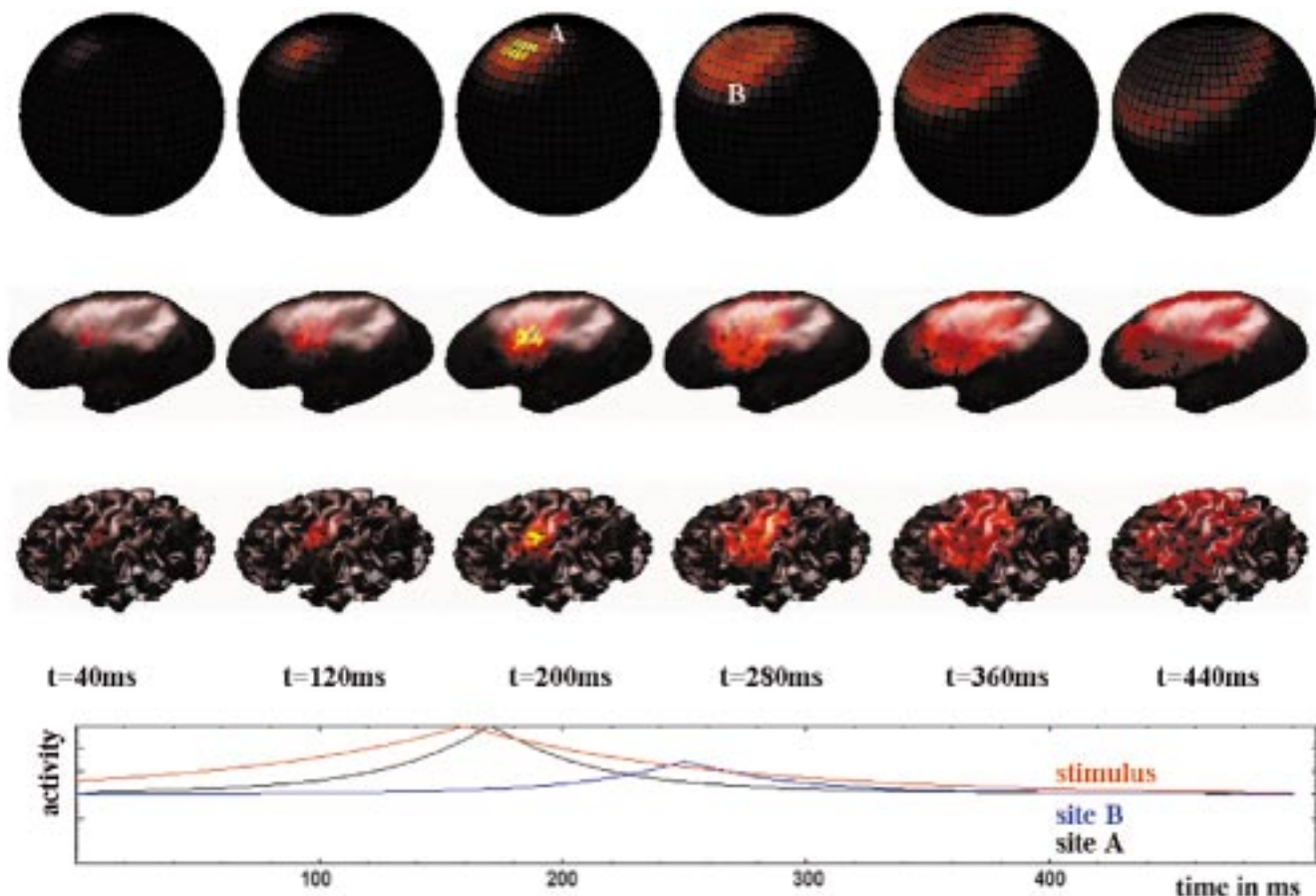


Fig. 5. The neural fields evoked by a transient stimulus distributed on the sphere (top row), inflated cortex (second row) and folded cortex (third row) for six separate time points. The bottom panel shows the time course of the stimulus (red line) and the activation pattern for two individual sites on the spherical surface.

as hemodynamic responses as measured by the fMRI provide other ways to restrict the range of allowable inverse solutions (see [4] for a recent review).

IV. SIMULTANEOUS CORTICAL AND EEG/MEG DYNAMICS

To illustrate the simultaneously on-going dynamics on the different levels of organization, that is, from ensembles to a pattern of cortical activity and finally to macroscopic measures such as EEG and MEG, we choose a simple example of induced wave propagation along the cortical sheet. The connectivity is spatially homogeneous and has an exponential falloff. Only one functional unit, activated by the stimulus input, is defined just anterior to the central sulcus, otherwise the neural sheet is completely homogeneous and isotropic. For visualization purposes, only one hemisphere is shown. The following numerical values are used in the simulation: radius $r_0 = 2$ of the cortical surface Γ , speed $v = 3$, connectivity function $f(x - X) = (2\pi\sigma^2)^{-1} \exp(-|x - X|/\sigma)$ and connectivity length $\sigma = 0.6$, sigmoid function $S[n] = (1 + \exp(-4n))^{-1} - 1/2$, and localization of stimulus input $\beta(x - x_0) = \exp(-|x - x_0|/\sigma_0)$ with $\sigma_0 = 0.05$. Spatial units refer to 0.1 m and time units to 100 ms.

At time $t = 0$, a stimulus signal $r(t)$ is introduced at $x = x_0$ in the cortical sheet Γ following (17). Here, the convolutive filter of (17) is set to $f(t - \tau) = \delta(t - \tau)$ where $\delta(t - \tau)$ is the Dirac delta function. In practical applications, such as evoked

potential and evoked field studies, the filter $f(t - \tau)$ has to be estimated. In the present case, the functional unit $p(x, t)$ of (17) has the same time course as the stimulus signal $r(t)$ which is an exponential increase until $t = 160$ ms, then followed by an exponential decrease (plotted on the bottom of Fig. 5). The stimulus excites the neural sheet at site A , $x = x_0$ and initiates wave propagation by means of a circular traveling wave front undergoing attenuation in space and in time. The time courses of the neural ensembles at site A and site B , which is more distant to the stimulus site, are shown. For several selected time points the spatiotemporal activity patterns on the sphere are plotted in the top row of Fig. 5. Here, and in the following the color code represents $-\text{MAX}$ to MAX as blue goes through black to red and yellow. In the rows below, the same neural activity patterns are represented on the unfolded cortex and on the folded cortex for the same time points after being mapped from the spherical representation following Sections III-D and III-E. Note that the circular traveling wave structure is preserved in both, the folded cortical and the spherical coordinate system implying that the error caused by the nonconformal coordinate transformation is not very significant, at least for the present case of purely homogeneous connectivity.

For purposes of calculation of the forward EEG and MEG solutions, we use a single layer head model (skull-brain) as defined in Section III-F and a spherical head shape. The 3-D current distribution is defined on the folded cortical surface located

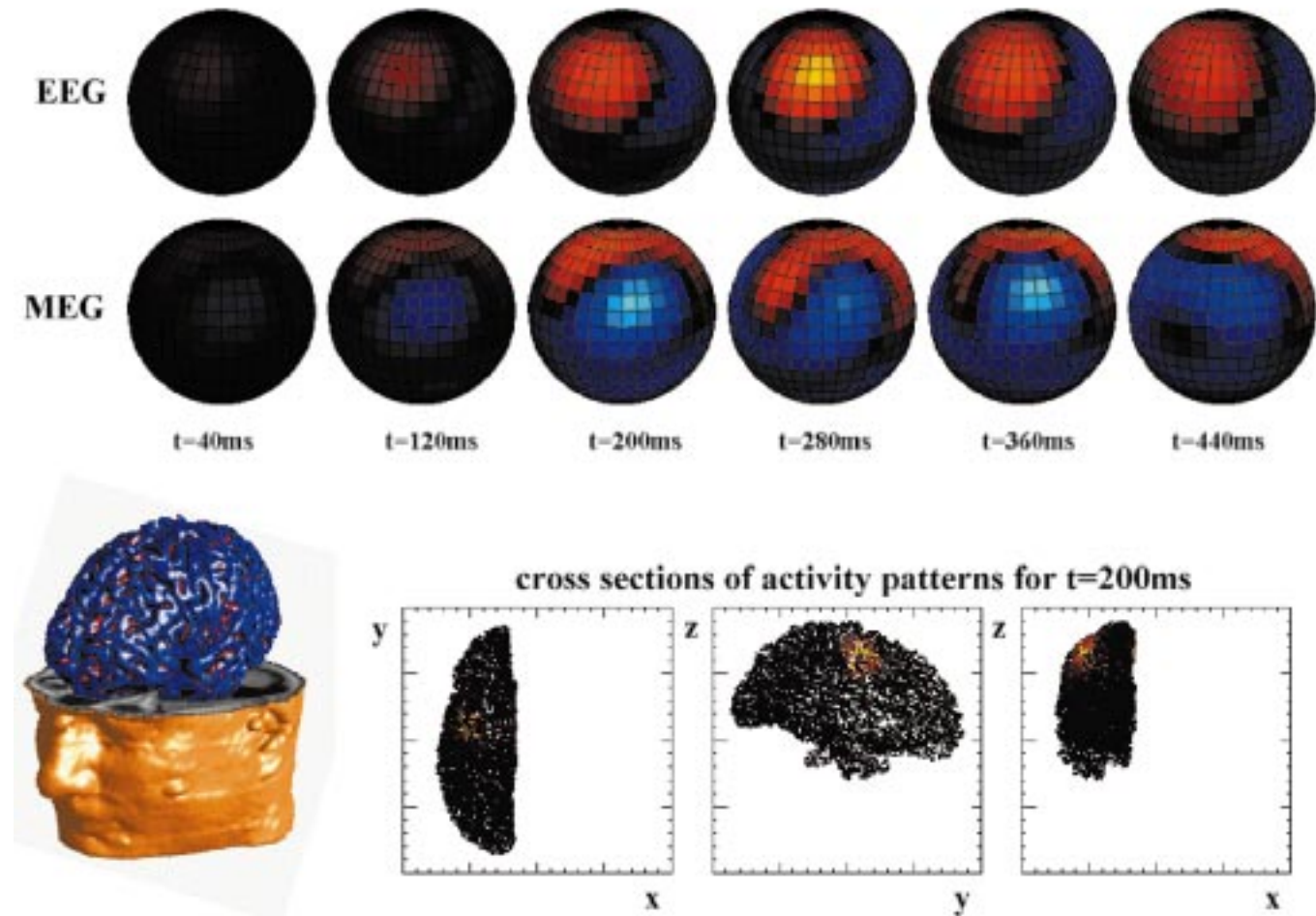


Fig. 6. The EEG (top row) and MEG (second row) forward solutions calculated at the same six time points as shown in Fig. 5. The activation patterns are plotted on a spherical head model used in the forward calculation (10 cm diameter). The spherical head model is oriented such that the nose is to the left of the page and the left side of the head is facing the reader. The location of the left cortical hemisphere used here is given within both the head of the subject (bottom left) and within the spherical model of the head (three views on the bottom right).

within the skull as illustrated on the bottom in Fig. 6 (upper skull surface is not shown). The color coding on the cortical surface reflects the local curvature at the vertices with blue and red indicating convex and concave curvature, respectively. Note that the cerebellum is not part of these surfaces and has been removed. Adjacent are plotted the three cross sections of the voxel distributions showing the neural activity pattern color coded for $t = 200$ ms. EEG and MEG detectors are placed directly on the spherical skull surface, infinitesimally close to each other. In this study, we use 100 EEG electrodes and 100 MEG detectors. For MEG, we assume radial gradiometers measuring the radial component of the magnetic field \mathbf{B} . We calculate the forward solutions of the EEG and MEG measured by these detectors following (20) and (21) and plot the resulting EEG (top row) and MEG (second row) patterns for the selected times. Note that the visualization is within the spherical system, the nose pointing to the left, basically resembling the perspective shown in the picture on the bottom left of Fig. 6. In both patterns, EEG and MEG, a dipolar structure emerges with a maximum activity at around 280 ms for the EEG and two maxima for MEG at around 200 and 360 ms. From Fig. 5 it is clear that the neural current

distribution is damped and flattens out as time evolves. However, the propagation of the neural wave front along the cortical surface is such that the neuromagnetic forward solution not only undergoes a spatial reorganization from 360 ms to 440 ms, but also a temporal organization which does not map trivially on the neural field activity.

It should be emphasized that the model presented here is not a form of inverse solution that defines putative neural sources associated with a particular experimental design and set of data. The mapping of neural fields onto the folded cortex and the calculation of the forward solution are performed for the purpose of connecting cortical dynamics with neurophysiological and behavioral findings. However, inverse solution techniques are most important for the proper localization of individual functional units on the folded cortical surface. Thereafter, the spatiotemporal data that result from the model are purely a function of the dynamics of the defined system and are not constrained by observed data anymore. It is possible therefore, to define a single dynamic model that can explain several different phenomena that may arise by changing input/output patterns. That is, once a model's components such as geometry, cortical and skull sur-

face, functional units and connectivity are established, then the same model may generate qualitatively different data given different types of inputs or different output constraints. For example, the theoretical and numerical study of impairments of functional units will eventually become possible on the cortical level, as well as on the levels of EEG/MEG and behavior.

V. FINAL REMARKS AND FUTURE DIRECTIONS

Here, we present a conceptual and methodological framework for the development of a theoretical model of human brain function and behavior that operates at multiple levels of description. Interconnected neural ensembles with homogeneous connections represent a neural level, while a network or systems level is defined by the interaction between heterogeneously connected cortical regions. An even broader level is defined by the computation of the spatiotemporal dynamics of EEG and MEG generated by the model and the connection of these data to behavioral dynamics. For concreteness: what is the neural substrate of the coupling between left and right finger within the bimanual coordination paradigm? Heterogeneous fiber tracts that connect the cortical, subcortical and spinal subsystems involved in coordination tasks still have to be implemented in our platform. These pathways couple the subsystems and, thus, add to their crosstalk and the resulting coordination dynamics. The heterogeneities introduce additional entries in the connectivity matrix of the neural field [38] carrying the information on distance and strength of coupling between areas. In the near future, developing technologies, such as diffusion tensor-weighted imaging, promise to provide complete information of the white matter tracts in the connectivity matrix of individual subjects [5], [56]. Developmental studies have reported that mirror movements appear as normal phenomena in young children; such mirror movements occur as mirror reversals of an intended movement on the other side of the body and disappear after the first decade of life, coinciding with the completion of myelination within the corpus callosum [9], [70] and implying the involvement of callosal fibers in bimanual crosstalk. These fibers are known to transmit both inhibitory and excitatory influences [52] and are generally topographic, that is, they go to homologous points in the contralateral hemisphere. Also, the involvement of subcortical structures and additional cortical areas during coordination is known. For example, the cerebellum is activated ipsilaterally during unimanual finger movements, but sometimes bilaterally recruited during sequential unimanual movements [28]. Supplementary motor areas also show increased activation (fMRI [29] and positron emission tomography [58]) for bimanual than for unimanual activity.

This collection of neurophysiological and anatomical facts provides evidence for the neural structures which support the coupling that mediates the information transfer during coordination, e.g., callosal fibers and cerebellar contributions. The challenge is to identify the anatomical basis contributing to the neuronal and behavioral dynamics. On the other hand, from the dynamics' perspective there are the descriptions and laws of coordination on selected levels of organization: the dynamics of the behavioral patterns and the dynamics of the corresponding EEG and MEG patterns. A description in terms of neuronal

activity patterns aids in developing the first contacts between generic pattern formation mechanisms and physiological quantities. The 3-D basis, developed throughout this paper, finally sets the stage on which noninvasive brain imaging techniques, theory and modeling, as well as spatiotemporal data analysis merge together to address questions in behavioral neuroscience.

ACKNOWLEDGMENT

The authors would like to thank J. Duncan for helpful comments on the transformation from the spherical to the cortical system.

REFERENCES

- [1] D. G. Albrecht and D. B. Hamilton, "Striate cortex of monkey and cat: Contrast response function," *J. Neurophys.*, vol. 48, pp. 217–237, 1989.
- [2] S. Amari, "Dynamics of pattern formation in lateral-inhibition type neural fields," *Biol. Cybern.*, vol. 27, pp. 77–87, 1977.
- [3] C. G. Assisi, V. K. Jirsa, and J. A. S. Kelso, "Dynamics of multifrequency coordination using parametric driving," *J. Sport Exer. Psych. Suppl.*, vol. 23, p. 95, 2001.
- [4] S. Baillet, J. C. Mosher, and R. M. Leahy, "Electromagnetic brain mapping," *IEEE Signal Proc. Mag.*, pp. 14–30, Nov. 2001.
- [5] P. G. Batchelor, D. L. G. Hill, F. Calamante, and D. Atkinson, "Study of connectivity in the brain using the full diffusion tensor from MRI," in *Lecture Notes in Computer Science*, M. F. Insana and R. M. Leahy, Eds. Berlin, Germany: Springer, 2001, Information Processing in Medical Imaging, pp. 120–133.
- [6] V. Braitenberg and A. Schüz, *Anatomy of the Cortex. Statistics and Geometry*. Berlin, Germany: Springer, 1991.
- [7] L. Borland and H. Haken, "Unbiased determination of forces causing observed processes. The case of additive and weak multiplicative noise," *Z. Phys. B—Condensed Matter*, vol. 81, p. 95, 1992.
- [8] L. Borland, "Learning the dynamics of two-dimensional stochastic Markov processes," *Open Syst. Inform. Dyn.*, vol. 1, p. 3, 1992.
- [9] K. Conolly and P. Stratton, "Developmental changes in associated movements," *Dev. Med. Child. Neurol.*, vol. 10, pp. 49–56, 1968.
- [10] A. Dale, B. Fischl, and M. I. Sereno, "Cortical surface-based analysis I," *Neuroimage*, vol. 9, pp. 179–194, 1999.
- [11] B. Ermentrout, "Neural networks as spatio-temporal pattern-forming systems," *Rep. Prog. Phys.*, vol. 61, pp. 353–430, 1998.
- [12] B. Fischl, M. I. Sereno, and A. Dale, "Cortical surface-based analysis II," *Neuroimage*, vol. 9, pp. 195–207, 1999.
- [13] D. J. Felleman and D. C. Van Essen, "Distributed hierarchical processing in the primate cerebral cortex," *Cereb. Cortex*, vol. 1, pp. 1–47, 1999.
- [14] P. Fink, P. Foo, V. K. Jirsa, and J. A. S. Kelso, "Local and global stabilization of coordination by sensory information," *Exp. Brain Res.*, vol. 134, pp. 9–20, 2000.
- [15] T. D. Frank, A. Daffertshofer, C. E. Peper, P. J. Beek, and H. Haken, "Toward a comprehensive theory of brain activity: Coupled oscillator systems under external forces," *Physica D*, vol. 144, pp. 62–86, 2000.
- [16] W. J. Freeman, "Tutorial on neurobiology: From single neurons to brain chaos," *Int. J. Bifurc. Chaos*, vol. 2, pp. 451–482, 1992.
- [17] A. Fuchs, J. A. S. Kelso, and H. Haken, "Phase transitions in the human brain: Spatial mode dynamics," *Int. J. Bifurc. Chaos*, vol. 2, pp. 917–939, 1992.
- [18] A. Fuchs, V. K. Jirsa, and J. A. S. Kelso, "Theory of the relation between human brain activity (MEG) and hand movements," *Neuroimage*, vol. 11, pp. 359–369, 2000.
- [19] A. Fuchs, J. M. Mayville, D. Cheyne, H. Weinberg, L. Deecke, and J. A. S. Kelso, "Spatiotemporal analysis of neuromagnetic events underlying the emergence of coordinative instabilities," *Neuroimage*, vol. 12, pp. 71–84, 2000.
- [20] H. Haken, *Synergetics. An Introduction*, 3rd ed. Berlin, Germany: Springer, 1983.
- [21] H. Haken, J. A. S. Kelso, and H. Bunz, "A theoretical model of phase transitions in human hand movements," *Biol. Cybern.*, vol. 51, pp. 347–356, 1985.
- [22] H. Haken, *Advanced Synergetics*, 2nd ed. Berlin, Germany: Springer, 1987.
- [23] —, *Principles of Brain Functioning*. Berlin, Germany: Springer, 1996.

- [24] —, "What can synergetics contribute to the understanding of brain functioning?," in *Analysis of Neurophysiological Brain Functioning*, C. Uhl, Ed. Berlin, Germany: Springer, 1999.
- [25] J. Hale and H. Kocak, *Dynamics and Bifurcations*. Berlin, Germany: Springer, 1996.
- [26] M. Hämmäläinen and J. Sarvas, "Realistic conductivity geometry model of the human head for interpretation of neuromagnetic data," *IEEE Trans. Biomed. Eng.*, vol. 36, pp. 165–171, Feb. 1989.
- [27] M. Hämmäläinen, R. Hari, R. J. Ilmoniemi, J. Knuutila, and O. V. Lounasmaa, "Magnetoencephalography—Theory, instrumentation and applications to noninvasive studies of the working human brain," *Rev. Mod. Phys.*, vol. 65, no. 2, pp. 413–497, 1993.
- [28] R. Ivry, "Cerebellar timing systems. Cerebellum and cognition," *Int. Rev. Neurobio.*, vol. 41, pp. 555–573, 1997.
- [29] L. Jäncke, M. Peters, M. Himmelbach, T. Nössel, J. Shah, and H. Steinmetz, "fMRI study of bimanual coordination," *Neuropsychologia*, vol. 38, pp. 164–174, 2000.
- [30] K. J. Jantzen, A. Fuchs, J. Mayville, L. Deecke, and J. A. S. Kelso, "Alpha and beta band changes in MEG reflect learning induced increases in coordinative stability," *J. Clin. Neurophys.*, vol. 112, pp. 1685–1697, 2001.
- [31] V. K. Jirsa, R. Friedrich, H. Haken, and J. A. S. Kelso, "A theoretical model of phase transitions in the human brain," *Biol. Cybern.*, vol. 71, pp. 27–35, 1994.
- [32] V. K. Jirsa, R. Friedrich, and H. Haken, "Reconstruction of the spatio-temporal dynamics of a human magnetoencephalogram," *Physica D*, vol. 89, pp. 100–122, 1995.
- [33] V. K. Jirsa and H. Haken, "Field theory of electromagnetic brain activity," *Phys. Rev. Lett.*, vol. 77, pp. 960–963, 1996.
- [34] —, "A derivation of a macroscopic field theory of the brain from the quasimicroscopic neural dynamics," *Physica D*, vol. 99, pp. 503–526, 1997.
- [35] V. K. Jirsa, A. Fuchs, and J. A. S. Kelso, "Connecting cortical and behavioral dynamics: Bimanual coordination," *Neur. Comput.*, vol. 10, pp. 2019–2045, 1998.
- [36] V. K. Jirsa, P. Fink, P. Foo, and J. A. S. Kelso, "Parametric stabilization of biological coordination: A theoretical model," *J. Biol. Phys.*, vol. 26, pp. 85–112, 2000.
- [37] V. K. Jirsa, "Dimension reduction in pattern forming systems with heterogeneous connection topologies," *Prog. Theo. Phys. Suppl.*, vol. 139, pp. 128–138, 2000.
- [38] V. K. Jirsa and J. A. S. Kelso, "Spatiotemporal pattern formation in neural systems with heterogeneous connection topologies," *Phys. Rev. E*, vol. 62, pp. 8462–8465, 2000.
- [39] J. A. S. Kelso, "On the oscillatory basis of movement," *Bull. Psychon. Soc.*, vol. 18, p. 63, 1981.
- [40] J. A. S. Kelso, S. L. Bressler, S. Buchanan, G. C. DeGuzman, M. Ding, A. Fuchs, and T. Holroyd, "A phase transition in human brain and behavior," *Phys. Lett. A*, vol. 169, pp. 134–144, 1992.
- [41] J. A. S. Kelso, *Dynamic Patterns. The Self-Organization of Brain and Behavior*. Cambridge, MA: MIT Press, 1995.
- [42] J. A. S. Kelso, V. K. Jirsa, and A. Fuchs, "Traversing scales of organization in brain and behavior (I, II, and III)," in *Analysis of Neurophysiological Brain Functioning*, C. Uhl, Ed. Berlin, Germany: Springer, 1999, pp. 73–125.
- [43] J. A. S. Kelso, A. Fuchs, R. Lancaster, T. Holroyd, D. Cheyne, and H. Weinberg, "Dynamic cortical activity in the human brain reveals motor equivalence," *Nature*, vol. 23, pp. 814–818, 1998.
- [44] K. Knuth, "A Bayesian approach to source separation," in *Proc. 1st Int. Workshop Independent Component Analysis and Signal Separation*, J. F. Cardoso, C. Jutten, and P. Loubaton, Eds., 1999, pp. 283–288.
- [45] Y. Kuramoto, *Chemical Oscillations, Waves and Turbulence*. Berlin, Germany: Springer, 1984.
- [46] J. Kwapien, S. Drozd, L. C. Liu, and A. A. Ioannides, "Cooperative dynamics in auditory brain response," *Phys. Rev. E*, vol. 58, pp. 6359–6367, 1998.
- [47] F. Kwasiok, "The reduction of complex dynamical systems using principal interaction patterns," *Physica D*, vol. 92, pp. 28–60, 1996.
- [48] —, "Optimal Galerkin approximations of partial differential equations using principal interaction patterns," *Phys. Rev. E*, vol. 55, pp. 5365–5375, 1997.
- [49] D. T. J. Liley, P. J. Cadusch, and J. J. Wright, "A continuum theory of electrocortical activity," *Neurocomputing*, vol. 26–27, p. 795, 1999.
- [50] S. Makeig, A. J. Bell, T. P. Jung, and T. J. Sejnowski, "Independent component analysis of electroencephalic data," in *Advances in Neural Information Processing Systems*, D. Touretsky, M. Mozer, and M. Hasselmo, Eds. Cambridge, MA: MIT Press, 1996, vol. 8, pp. 145–151.
- [51] J. M. Mayville, S. L. Bressler, A. Fuchs, and J. A. S. Kelso, "Spatiotemporal reorganization of electrical activity in the human brain associated with timing transition in rhythmic auditory-motor coordination," *Exp. Brain Res.*, vol. 127, pp. 371–381, 1999.
- [52] U. M. Meyer, S. Röricht, H. von Einsiedel, F. Kruggel, and A. Weindl, "Inhibitory and excitatory interhemispheric transfers between motor cortical areas in normal humans and patients with abnormalities of corpus callosum," *Brain*, vol. 118, pp. 429–440, 1995.
- [53] J. C. Mosher, S. Baillet, and R. M. Leahy, "EEG source localization and imaging using multiple signal classification approaches," *J. Clin. Neurophys.*, vol. 16, pp. 225–238, 1999.
- [54] P. L. Nunez, "The brain wave equation: A model for the EEG," *Math. Biosci.*, vol. 21, pp. 279–297, 1974.
- [55] —, *Neocortical Dynamics and Human EEG Rhythms*. Oxford, U.K.: Oxford Univ. Press, 1995.
- [56] G. J. M. Parker, C. A. M. Wheeler-Kingshott, and G. J. Barker, "Distributed anatomical brain connectivity derived from diffusion tensor imaging," in *Information Processing in Medical Imaging*, M. F. Insana and R. M. Leahy, Eds, Germany: Springer, 2001, Lecture Notes in Computer Science, pp. 106–120.
- [57] P. A. Robinson, C. J. Rennie, and J. J. Wright, "Propagation and stability of waves of electrical activity in the cerebral cortex," *Phys. Rev. E*, vol. 56, p. 826, 1997.
- [58] N. Sadato, Y. Yonekura, A. Waki, A. Yamada, and Y. Ishii, "Role of the supplementary motor area and the right premotor cortex in the coordination of bimanual finger movements," *J. Neurosci.*, vol. 17, pp. 9667–9674, 1997.
- [59] M. Schetzen, *The Volterra and Wiener Theories of Nonlinear Systems*. Melbourne, FL: Krieger, 1989.
- [60] G. Sclar, J. H. R. Maunsell, and P. Lennie, "Coding of image contrast in central visual pathways of the macaque monkey," *Vis. Res.*, vol. 30, pp. 1–10, 1990.
- [61] M. L. Steyn-Ross, D. A. Steyn-Ross, J. W. Sleight, and D. T. J. Liley, "Theoretical EEG stationary spectrum for a white-noise-driven cortex," *Phys. Rev. E*, vol. 60, p. 7299, 1999.
- [62] C. D. Tesche, M. A. Uusitalo, R. J. Ilmoniemi, M. Huottilainen, M. Kajola, and O. Salonen, "Signal-space projections of MEG data characterize both distributed and well-localized neuronal sources," *Electroenceph. Clin. Neurophysiol.*, vol. 95, pp. 189–200, 1995.
- [63] C. Uhl, R. Friedrich, and H. Haken, "Analysis of spatio-temporal signals of complex systems," *Phys. Rev. E*, vol. 51, pp. 3890–3900, 1995.
- [64] C. Uhl, Ed., *Analysis of Neurophysiological Brain Functioning*. Berlin, Germany: Springer, 1999.
- [65] G. V. Wallenstein, J. A. S. Kelso, and S. L. Bressler, "Phase transitions in spatiotemporal patterns of brain activity and behavior," *Physica D*, vol. 84, pp. 626–634, 1995.
- [66] S. J. Williamson and L. Kaufman, "Analysis of neuromagnetic signals," in *Methods of Analysis of Brain Electrical and Magnetic Signals. EEG Handbook*, A. S. Gevins and A. Remond, Eds. Amsterdam, The Netherlands: Elsevier Science, 1987.
- [67] H. R. Wilson and J. D. Cowan, "Excitatory and inhibitory interactions in localized populations of model neurons," *Biophys. J.*, vol. 12, pp. 1–24, 1972.
- [68] —, "A mathematical theory of the functional dynamics of cortical and thalamic nervous tissue," *Kybernetik*, vol. 13, pp. 55–80, 1973.
- [69] J. J. Wright and D. T. J. Liley, "Dynamics of the brain at global and microscopic scales: Neural networks and the EEG," *Behav. Brain Sci.*, vol. 19, p. 285, 1996.
- [70] P. I. Yakovlev and A. R. Lecours, "The myelogenetic cycles of regional maturation of the brain," in *Development of the Brain in Early Life*, A. Minkowski, Ed. Oxford, U.K.: Blackwell, 1967, pp. 3–70.